10^{th} International Conference on Fracture Mechanics of Concrete and Concrete Structures
FraMCoS-X
G. Pijaudier-Cabot, P. Grassl and C. La Borderie (Eds)
https://doi.org/10.21012/FC10.23554

CLUSTERING OF ACOUSTIC EMISSION SIGNALS FOR FRACTURE MONITORING DURING ACCELERATED CORROSION OF REINFORCED CONCRETE PRISMS

CHARLOTTE VAN STEEN*, **MARTINE WEVERS**† **AND ELS VERSTRYNGE** ‡

*Department of Civil Engineering, KU Leuven
Leuven, Belgium
e-mail: charlotte.vansteen@kuleuven.be

†Department of Materials Engineering, KU Leuven
Leuven, Belgium
e-mail: martine.wevers@kuleuven.be

‡Department of Civil Engineering, KU Leuven
Leuven, Belgium
e-mail: els.verstrynge@kuleuven.be

Key words: Reinforcement corrosion, Acoustic Emission, Signal Analysis, Fracture, Localisation, Clustering

Abstract. Corrosion of the reinforcement is one of the major deterioration mechanisms in existing reinforced concrete (RC) structures causing considerable costs for maintenance and repair. The development of reliable tools to localise and characterise such damage is essential to assess the structural capacity. This paper investigates the use of the acoustic emission (AE) technique during an accelerated corrosion process of reinforced concrete prisms. AE monitoring was performed continuously during the corrosion process using six sensors to allow localisation of the AE events in 3D. A sample with and without a stirrup was tested. An AE testing and post-processing protocol was developed and will be discussed in this paper. A signal-based clustering algorithm was developed to distinguish different AE sources from each other. Results show that damage could be localised correctly in both samples. Different types of signals could be distinguished by the clustering algorithm. This was compared with crack width measurements, time of arrival, location and RA-AF analysis. It was concluded that mainly concrete cracking was recorded and localised by AE sensing in both samples.

1 INTRODUCTION

One of the deterioration mechanisms that seriously threatens the durability of our existing reinforced concrete (RC) structures is corrosion. Due to either carbonation and/or chlorides, steel is consumed and turned into expansive corrosion products. These products cause internal tensile stresses in the concrete and will eventually cause cracking and spalling.

The most common inspection method on-site is visual inspection where the damage is assessed on the surface by taking pictures, hammer tapping and crack width measurements. This method provides insight in the cause and extent of the damage, however, only damage on the surface can be detected. Electrochemical techniques are also widely used, unfortunately they are dependent on climatic conditions and might lack to provide precise information [1][2]. This urges the need for the development of other techniques. Acoustic emission (AE) technique is very promising as it can capture the corrosion process itself, but also the progress of concrete cracking by detecting the high-frequency elastic waves that are emitted by the fracture process [3][4].

AE monitoring has been successfully applied during rebar corrosion in concrete and destructive testing of corroded RC samples and components [5][6]. In the literature, AE analysis is mainly performed based on AE parameters which are a set of extracted features that describe the signal. For corrosion monitoring, it allows to distinguish different stages during the process such as the initiation (before cracking) and propagation (after cracking) stage [7]. Unfortunately this approach is dependent on a user defined threshold which makes it hard to compare the results when having different setups.

Signal-based analysis can alter this as it takes into account the underlying modal structure of an AE signal. It can allow to distinguish different damage processes leading to a more reliable interpretation of the different damage mechanisms. It would give the end user the ability to tell which source mechanism is present and whether maintenance or repair is necessary. However, this approach poses some challenges as the transfer function of a signal is influenced by many aspects such as the couplant, sensor and system, but also the propagation path of the signal. It has been applied successfully in composites and in fibre reinforced concrete to make a distinction between fibre pull-out, matrix cracking and fibre failure [8][9], but has not been performed so far on corrosion in reinforced concrete.

To apply AE sensing reliably on-site, both AE source localisation and characterisation are important to assess a structure. In this paper, an AE testing and post-processing protocol is presented in order to reach this goal. A new signal-based clustering algorithm based on cross-correlation was developed by the authors and proven to be applicable on small scale samples [4]. In this paper, the clustering algorithm will be upscaled to reinforced concrete prisms.

2 EXPERIMENTAL PROCEDURE

2.1 Materials and specimen preparation

Two samples were compared in the current investigation: (1) one sample with a rebar in the center of the sample (sample A), and (2) a similar sample also having a corroding stirrup (sample B) (figure 1). A ribbed rebar (BE400) with a nominal diameter of 14 mm was placed horizontally in the center of the wooden mould (150x150x250 mm^3) and was protruding from both sides in order to connect the power supply for the accelerated corrosion afterwards. For the second sample, a smooth stirrup with a nominal diameter of 6 mm was placed around the main rebar and was electrically connected to it with a copper wire. The concrete composition is shown in table 1. The average compressive strength at 28 days, tested on cubes, was 55.04 MPa with a deviation of 3.19 MPa and the average flexural strength, tested on prisms, was 5.16 MPa with a deviation of 0.63 MPa. After curing for 28 days in a curing room (± 20°C, ± 95% RH), the specimens were fully immersed in a 5% sodium chloride solution for three days. Afterwards, the specimens were placed in the accelerated corrosion setup (figure 2) in a climatised room (± 20°C, ± 60% RH). The accelerated corrosion process and AE monitoring started at an age of 31 days.

Table 1: Concrete composition [kg/m^3].

CEM I 42.5N	Sand (0/5)	Aggregates (4:14)
350	620	1270
Water	Chlorides	W/C
164	7	0.46

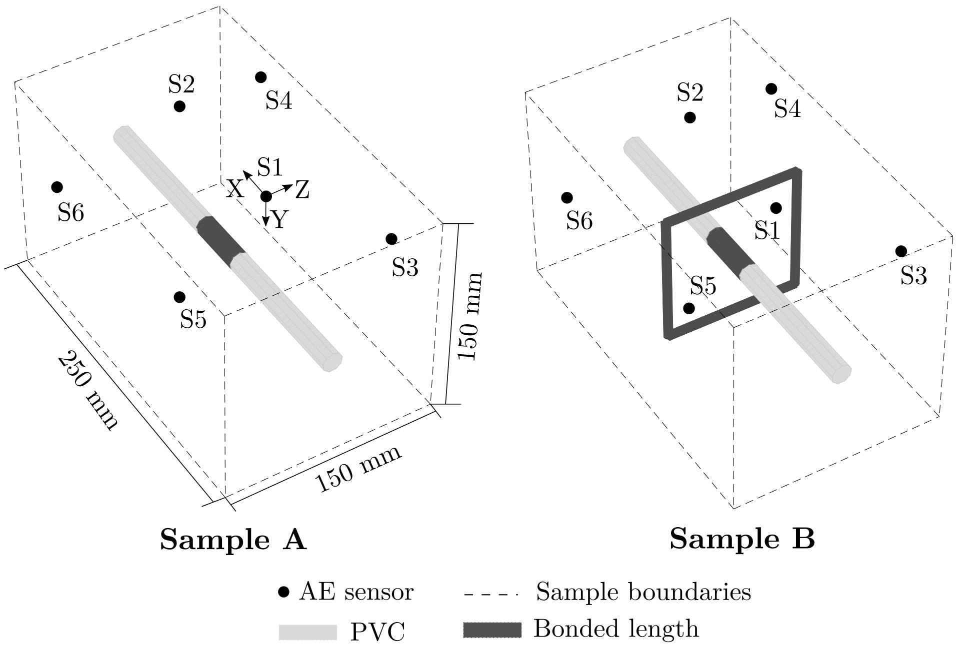

Figure 1: Sample layout and sensor arrangement for sample A and B.

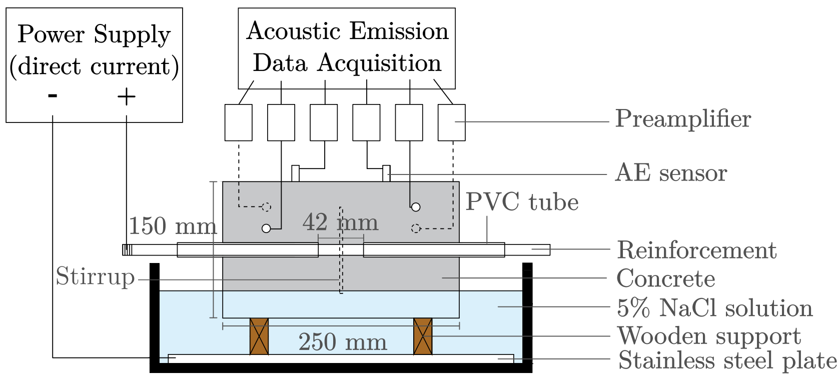

Figure 2: Accelerated corrosion setup.

2.2 Accelerated corrosion process

An imposed direct current was used to accelerate the corrosion process in the laboratory. A constant current density of 100 μA/cm^2 was chosen. The rebar acted as the anode and is thus connected to the positive side of the DC regulator. The negative side was connected to the cathode which was a stainless steel plate. The specimen was partially immersed in a 5% sodium chloride solution to ensure electrical connectivity and chloride ingress. The setup is shown in figure 2. Cracks were measured every week with a crack meter having an accuracy of 0.05 mm. The samples were corroded and AE were monitored continuously for two months.

2.3 Acoustic emission (AE) monitoring

AE monitoring was performed during the accelerated corrosion process with six piezoelectric sensors with a flat frequency response between 100-400 kHz. The six sensors were attached on the specimen surface with hot melt glue and connected to pre-amplifiers with a fixed gain of 34 dB. The sensor arrangement and coordinates are shown in figure 1 and table 2 respectively. The pre-amplifiers were connected to a Vallen AMSY-6 acquisition system with six AE channels. AE parameters and waveforms were stored on a PC and the Vallen VisualAE software was used to visualise the data in real time. Matlab was used for further processing. The first arrival time picking was done using a fixed threshold of 50 dB. This first estimation of the time of arrival (TOA) t_{first} was used to discretise different signals and store them afterwards. The stored signal had a total length of 200 μs including 20 μs before t_{first}.

Table 2: Sensor coordinates [mm].

Sensor	X	Y	Z
S1	0	0	0
S2	100	0	0
S3	-25	-50	75
S4	125	-25	75
S5	-25	-25	-75
S6	125	-50	-75

3 AE DATA POST-PROCESSING

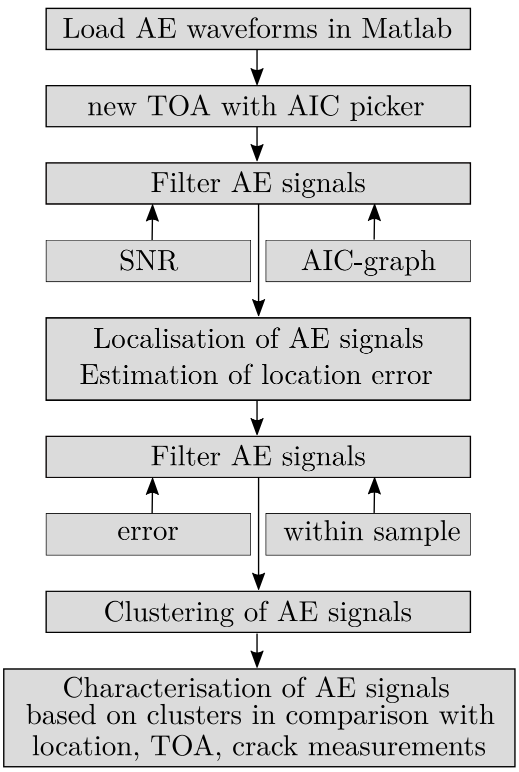

Figure 3: Flowchart of AE post-processing protocol.

In order to assign possible damage sources to the recorded AE signals, comparison with their source location can be helpful. Intensive filtering was needed in order to only keep the signals that will allow an accurate localisation. A post-processing protocol was developed and implemented in Matlab. The workflow is shown in figure 3.

3.1 Arrival time picking

A more exact TOA was determined using the Akaike Information Criterion (AIC) [10][11], as expressed in equation 3.1:

$$\begin{aligned}\text{AIC}(t_w) &= t_w \cdot \log_{10}(\text{var}(R_w(1,t_w))) + \cdots \\ &\quad \cdots (T_w - t_w - 1) \cdots \\ &\quad \cdots \cdot \log_{10}(\text{var}(R_w(t_w+1,T_w))),\end{aligned}$$

The signal R_w is divided into two sections at a point t_w. Point t_w ranges from 1 to T_w, with T_w the non-dimensional length of the time window. The term var$(R_w(1,t_w))$ is the variance function of all samples from 1 to t_w and var$(R_w(t_w+1,T_w))$ is the variance function of all samples from point t_w+1 to T_w. The absolute minimum of all values indicates the new onset time t_{AIC}.

Only the signals of which the TOA could be determined accurately were used for localisation. Two criteria were applied to estimate the accuracy. These criteria were presented by Gollob [12] and adapted in the current paper. The first criterion is based on the signal-to-noise ratio (SNR) which gives the ratio of the signal power S to the noise power N. S was defined as the maximum amplitude of the entire signal. N was defined as the maximum amplitude of the first 10 μs of the signal. Based on the recorded signals, SNR was set to 10. If the ratio was larger than 10, the difference between the actual signal and noise level was large enough and the signals were kept for further analysis. The second criterion enhances the shape of the AIC-value graph. The actual TOA was estimated accurately if t_{AIC} coincided with the first low point (local minimum) of the AIC-value graph. If this was not the case, the time difference between this first low point and t_{AIC} was checked.

It was found that if the time difference was less than 7 μs, or if the time difference was larger than 7 μs but the slope between the first low point and t_{AIC} was smaller than -25, the estimation with AIC was still found to be reasonably accurate. If none of the criteria were fulfilled, the signal was excluded from the analysis.

3.2 Localisation of AE events

For AE source localisation in 3D, Geiger's method was implemented in Matlab. Geiger's method is an iterative approach that computes the best approximation of the source location based on a least-squares approach [12][13]. At least four sensors are needed to solve the equations. In this paper, an homogeneous velocity model was used and a straight propagation path between source and sensor is assumed. The arrival time $t_{a,i}$ at the i^{th} sensor can be written as follows:

$$t_{a,i} = t_0 + \cdots$$
$$\cdots \frac{1}{v_p}\sqrt{(x_i - x_0)^2 + (y_i - y_0)^2 + (z_i - z_0)^2} \tag{1}$$

with x_0, y_0 and z_0 are the coordinates of an AE source, t_0 is the onset time or origin time of the source, x_i, y_i and z_i are the coordinates of the i^{th} sensor, and v_p is the wave velocity. The wave velocity was determined during calibration and set to 3950 mm/ms for sample A and 3980 mm/ms for sample B. A trial hypocenter (x_0, y_0, z_0, t_0) is needed as a first guess. The middle of the specimen was chosen as a first source location. The problem is overdetermined when there are more than four arrival times. For each sensor i there will be residuals γ_i between the observed TOA t_{ao} and calculated TOA t_{ac}:

$$\gamma_i = t_{ao} - t_{ac} \tag{2}$$

These residuals will be minimised by calculating and applying correction factors (δx, δy, δz, and δt) in order that the calculated arrival times best match the observed arrival times. The residuals can also be written as:

$$\gamma_i = \frac{\partial f_i}{\partial x}\delta x + \frac{\partial f_i}{\partial y}\delta y + \frac{\partial f_i}{\partial z}\delta z + \frac{\partial f_i}{\partial t}\delta t \tag{3}$$

where f_i is the right side of eq. 1. or in matrix notation:

$$\boldsymbol{\gamma} = \mathbf{A}\boldsymbol{\delta}\mathbf{corr} \tag{4}$$

where $\mathbf{A}$ is the matrix of partial derivatives and $\boldsymbol{\delta}\mathbf{corr}$ the correction vector. For four sensors, one unique solution exists. For more than four sensors, the problem is overdefined and the correction vector is calculated by the Moore-Penrose inverse to compute the least squares solution:

$$\boldsymbol{\delta}\mathbf{corr} = (\mathbf{A^T A})^{-1}\mathbf{A^T}\boldsymbol{\gamma} \tag{5}$$

The trial solution is updated at the beginning of each iteration step by adding the correction factor from the previous iteration:

$$\begin{aligned} x_o^{k+1} &= x_o^k + \delta x, \\ y_o^{k+1} &= y_o^k + \delta y, \\ y_o^{k+1} &= z_o^k + \delta z, \\ t_o^{k+1} &= t_o^k + \delta t \end{aligned}$$

Two criteria were set to stop the iterative process. The first stopping criterion is based on the size of the correction vector. The correction vector $\boldsymbol{\delta}\mathbf{corr}$ includes both spatial and time components which makes it difficult to calculate its size as it contains different units [13]. Therefore, the correction vector $\boldsymbol{\delta}\mathbf{d}$ was determined only based on the spatial components:

$$\boldsymbol{\delta}\mathbf{d} = \sqrt{\delta x^2 + \delta y^2 + \delta z^2} \tag{6}$$

The correction vector should be smaller than a chosen tolerance ϵ. When $\boldsymbol{\delta}\mathbf{d}$ goes to zero, it is a sign of convergency. Therefore the tolerance ϵ was chosen to be 0.02. The maximum amount of iterations was set to 50.

To visualise an estimation of the localisation accuracy, error ellipsoids can be used. Therefore, the covariance matrix $\mathbf{C}$ should be calculated:

$$\mathbf{C} = \sigma_d^2(\mathbf{A}^T\mathbf{A})^{-1} \tag{7}$$

where σ_d^2 is the data variance. Only spatial errors are of interest. $\mathbf{C}$ is thus a 3x3 matrix having the variances of the source parameters in direction of the three coordinates on its diagonal.

From the eigenvalues λ_i of $\mathbf{C}$, the length of the semi-axis can be determined. The eigenvectors v_i will describe the orientation. The semi-axes l_i for a 68%-ellipsoid are described as:

$$l_i = \sqrt{3.53\lambda_i} \tag{8}$$

The data variance σ_d is usually unknown. However, it is possible to estimate this based on the residuals by:

$$\sigma_d^2 = \frac{\sum_{i=1} \gamma_i^T \gamma_i}{m-q} \tag{9}$$

with m the observed arrival times and q the unknown source parameters which is 4 in this case (x, y, z, t). However it is reported by Schechinger [14] that this gives an overestimation of the error. Therefore, σ_d^2 is substituted by s with following equation:

$$s = \frac{\sum_{i=1} \gamma_i^T \gamma_i}{m} \tag{10}$$

3.3 Agglomerative hierarchical clustering based on cross-correlation

In Van Steen et al. [4], a signal-based clustering algorithm is elaborated that can be used to characterise different AE signals that originate during the corrosion test. Clustering is the process in which a set of objects or points are grouped into categories or clusters according to a virtual distance measure. Similar points in the same cluster will have a small distance to each other while points in different clusters are dissimilar and thus are at a large distance from one another. In signal-processing, normalised cross-correlation can be used as a measure of similarity of two signals. For continuous functions $f(t)$ and $g(t)$, the normalised cross-correlation is defined as:

$$\hat{R}_{fg}(t) = \frac{R_{fg}(t)}{\sqrt{R_{ff}(0)R_{gg}(0)}} \tag{11}$$

where

$$R_{fg}(t) = (f \star g)(t) = \int_{-\infty}^{+\infty} f(\tau)g(t+\tau)d\tau \tag{12}$$

$$R_{ff}(0) = \int_{-\infty}^{+\infty} f(\tau)^2 d\tau \tag{13}$$

$$R_{gg}(0) = \int_{-\infty}^{+\infty} g(\tau)^2 d\tau \tag{14}$$

A correlation coefficient $cc(f, g)$ between 0 and 1 can be defined as the maximum of the absolute value of all points (Eq. 15). The value 1 means that the two signals are identical whereas 0 means that they are not similar at all.

$$cc(f, g) = max(abs(\hat{R}_{fg}(t))) \tag{15}$$

Dissimilarity can be used as a virtual distance measure to cluster AE signals. The distance or dissimilarity $d(f, g)$ can be defined as 1 minus the correlation coefficient $cc(f, g)$. According to this definition, the more similar two signals are, the shorter their distance will be. The distance approaches 0 as correlation goes to 1. Each signal forms a separate cluster at the start. These one-signal-clusters are then combined into larger clusters based on their closeness. Two clusters with the shortest distance, i.e. smallest dissimilarity, are merged first. The distance between this newly formed cluster and the other existing clusters needs to be calculated first. The calculation of this inter-cluster distance or cophenetic distance can be executed in different ways, among which single (nearest neighbour), complete (furthest neighbour), and average linkage are most commonly used. Average linkage is used in this paper as single linkage can produce chain-shape clusters and complete linkage is more sensitive to outliers.

4 RESULTS AND DISCUSSION

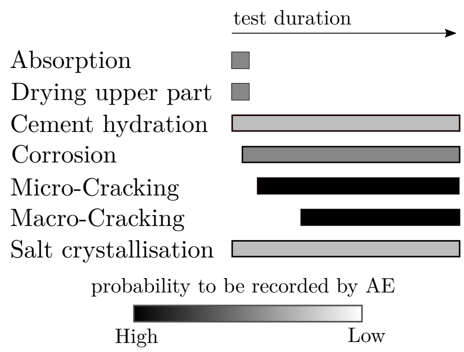

Figure 4: Possible AE sources.

A list of possible sources that could have been be captured by the AE technique were listed and the probability of their detection by AE sensing was estimated as shown in figure 4. Dummy samples were tested to eliminate some of these processes such as cement hydration (concrete block on a table) and absorption/drying (concrete block in water). Some signals were recorded due to absorption and drying of the concrete block. However, these were mainly single hits for which the arrival time could not be picked accurately. These signals would therefore be deleted automatically when filtering the data.

4.1 Sample A: longitudinal reinforcement, no stirrup

AE localisation results without filtering and arrival time picking by AIC are shown in figure 5. Localised events are very scattered and many reflections can be noticed in the top part of the sample. Characterising the damage sources would be impossible.

Figure 6 shows the results after running through the post-processing protocol, taking into account the events that are localised by 4, 5 or 6 channels and having an error of less than 20 mm in every direction of the error ellipsoid. Notice that the events localised by 4 sensors do not have an error ellipsoid as the solution is unique.

At the end of the experimental program, a crack could be noticed at the bottom side of the sample, perpendicular to the rebar. A small amount of events is localised near the crack at the bottom. The localisation results will be most accurate when the sensor array surrounds the area of interest. Due to the corrosion setup, it was necessary to place the sensors on top of the sample as it was impossible to attach the sensors in the salt solution. Therefore, this sensor layout is not ideal to monitor the cracks that will be formed at the bottom part of the sample. The wave will be reflected and attenuated before it reaches one of the sensors. Also the rebar has a big influence on the propagation path to sensor 1 and 2.

Also a crack at the side (surface where S5 and S6 where mounted) could be seen. This crack was parallel to the rebar and was localised succesfully as visualised on figure 6.

AE events are also localised at the side of S3 and S4. However, no crack could be seen on this surface. It is possible that a crack was growing, but did not reach the surface yet.

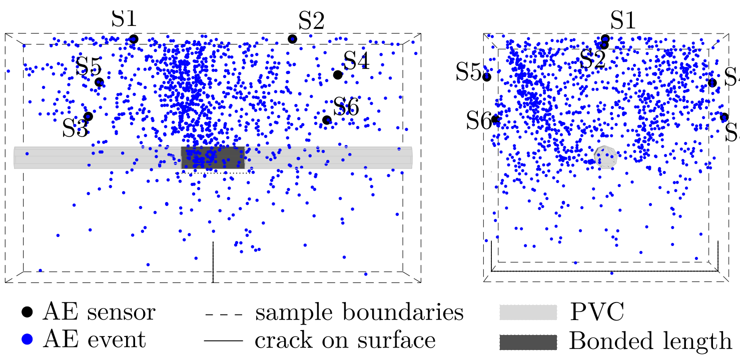

Figure 5: Unfiltered localised events.

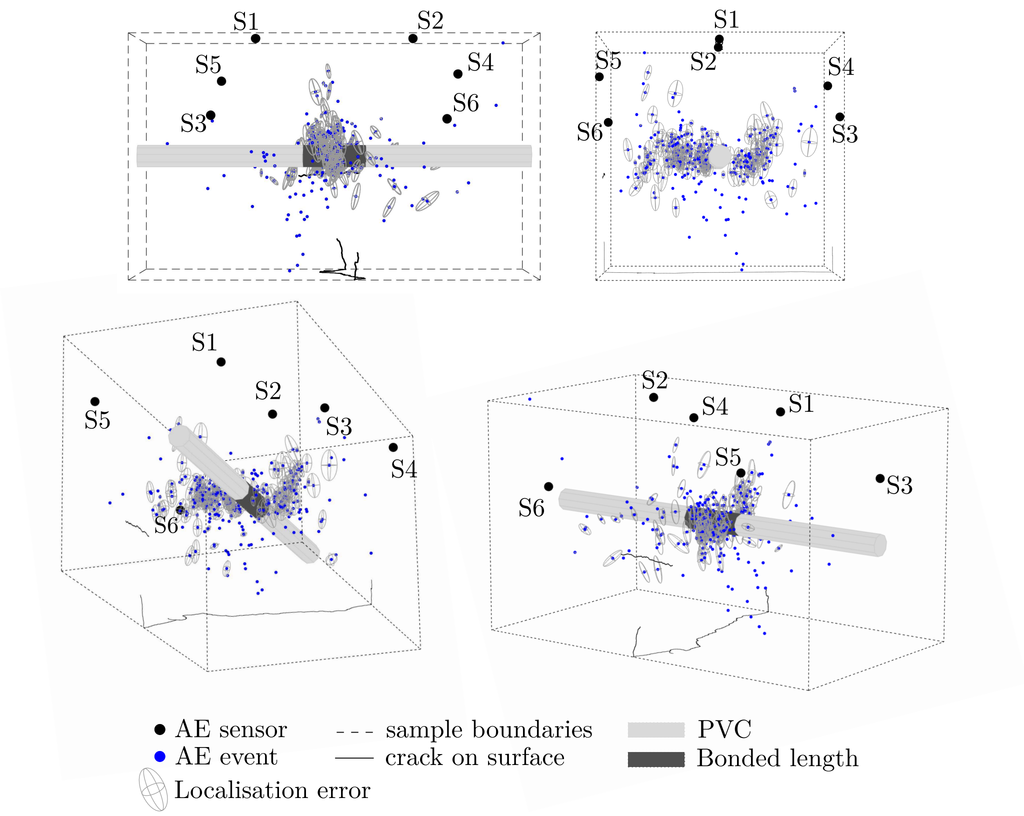

Figure 6: Localisation results of sample A with indication of the error ellipses and cracks that were visible on the sample surface.

The results of the clustering algorithm are shown in figure 7. The threshold was set to 0.7 as reported previously in Van Steen et al. [4] and verified by clustering signals from artificial sources. Two clusters can be distinguished. The largest one (red, cluster 1) contains signals with a peak frequency between 200 and 250 kHz. The smallest cluster (green, cluster 2) contains only three signals having a peak frequency around 100 kHz.

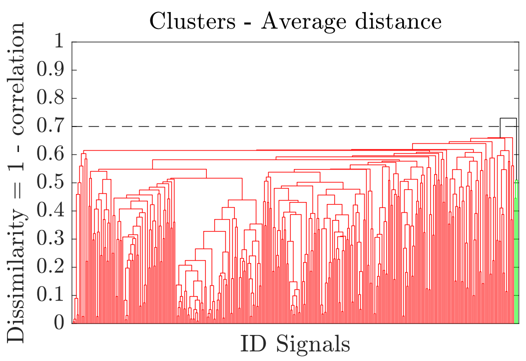

Figure 7: Sample A: Dendrogram showing two different clusters.

The signals of cluster 1 are recorded almost from the beginning of the test as shown in figure 8. To investigate whether this process could be corrosion or concrete cracking, an RA-AF analysis was carried out. The difference between a shear crack and a tensile crack is defined through the RA value (Rise Time divided by Amplitude) and average frequency (Counts divided by Duration). For the latter, the same frequency over the entire duration of the signal is assumed without performing a Fast Fourier Transform (FFT). Higher frequencies and lower RA-values are typically assigned to the tensile mode (cracking) whereas lower frequencies and higher RA-values to the shear mode (in our case corrosion, see [4][6]). As presented in figure 9, most signals are assigned to the tensile mode. Therefore it can be concluded that cluster 1 is cracking of the concrete cover. As only three signals are assigned to cluster 2, it is hard to assign a damage source. Cluster 2 might be corrosion as this is typically a lower frequent signal in comparison with concrete cracking [15]. There may be two reasons why few signals are captured. On the one hand because of the large thickness of the concrete cover leading to the signal being attenuated before it reaches the sensor. On the other hand because of the frequency range of the system and sensors which was between 95 kHz and 850 kHz and between 100 and 400 kHz respectively.

Figure 10 shows the cumulative AE energy versus time in comparison with the crack measurements. The time frame where the cracks must have reached the surface is indicated by a grey area. The moment at which internal cracking is initiated can typically be distinguished by a sudden jump in the AE energy curve [16]. Based on figure 10 this must have been around day 12. However, on figure 8 some low energy events can alredy be noticed before day 12. This might be some initial micro-cracking.

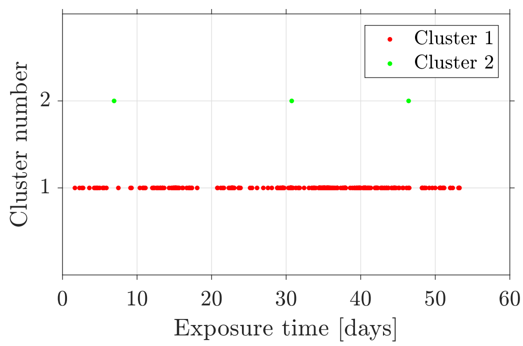

Figure 8: Sample A: Events of different clusters versus time.

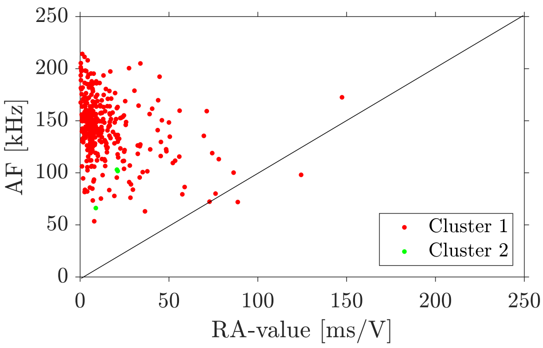

Figure 9: Sample A: Relationship between RA-value and AF of clustered events.

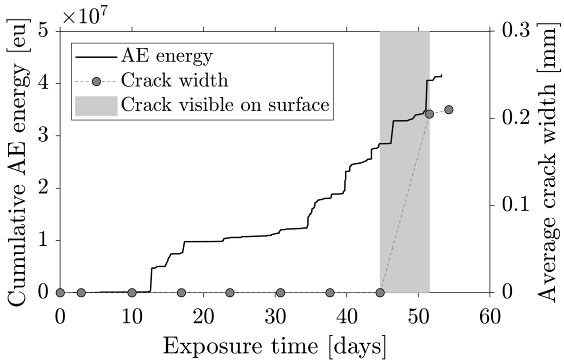

Figure 10: Sample A: Time history of AE energy in comparison with average crack width.

4.2 Sample B: longitudinal reinforcement and stirrup

The same analysis was performed for sample B. This sample already showed a small shrinkage crack at the beginning of the test. Most AE events are localised around the stirrup at the side where the crack was visible on the surface. This is shown in figure 11. Also for this sample, a large cluster (red, cluster 1) and smaller cluster (green, cluster 2) were distinguished by the clustering algorithm (figure 12). A third cluster (blue, cluster 3) can also be noticed. Again peak frequencies range between 200 and 250 kHz for cluster 1 and around 100 kHz for cluster 2. Cluster 3 only contains 2 signals having a peak frequency around 180 kHz. A RA-AF analysis was also carried out for sample B (figure 13). As was the case for sample A, the signals of sample B can mainly be assigned to the tensile mode meaning that cluster 1 is cracking of the concrete cover. Events are mainly recorded starting from day 20 (figure 8) when the crack started to grow (figure 15). Also for this sample it is hard to assign a specific damage source to cluster 2 and cluster 3 as few events were localised.

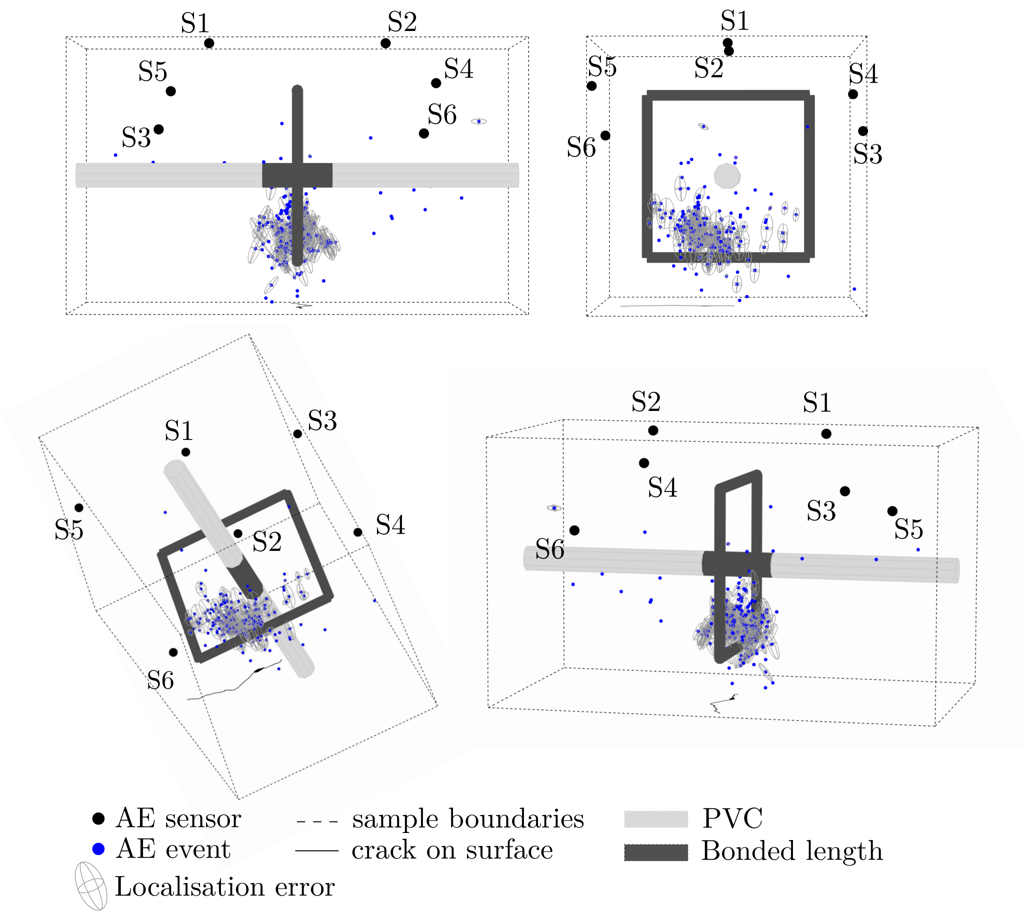

Figure 11: Localisation results of sample B with indication of the error ellipses and crack that was visible on the sample surface.

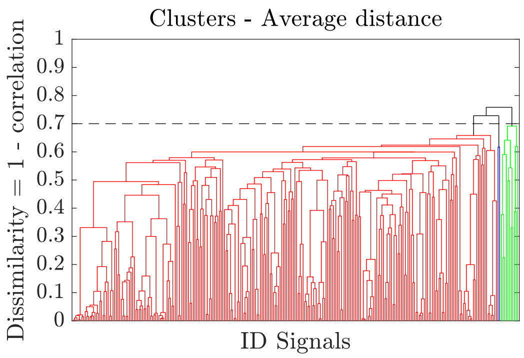

Figure 12: Sample B: Dendrogram showing three different clusters.

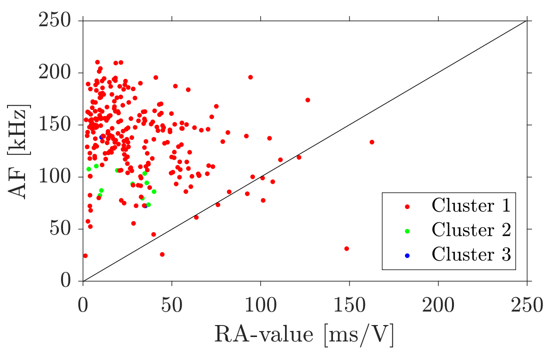

Figure 13: Sample B: Relationship between RA-value and AF of clustered events.

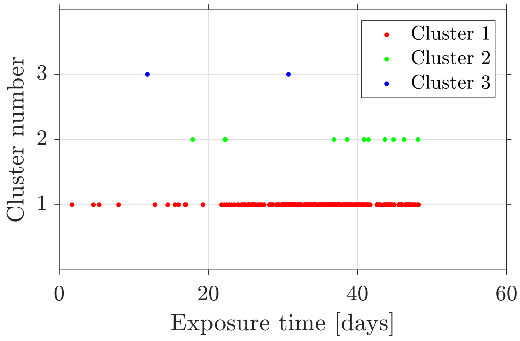

Figure 14: Sample B: Events of different clusters versus time.

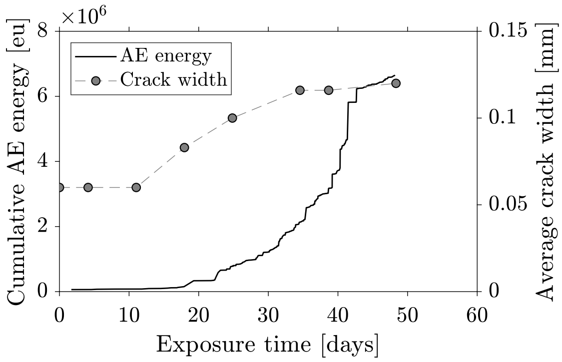

Figure 15: Sample B: Time history of AE energy in comparison with average crack width.

4.3 AE post-processing protocol: evaluation

In this last section some important parameters are discussed which could improve testing and analysis. First of all, the sensor layout is very important in order to be able accurately localise AE events. Due to the corrosion setup, it was not possible to put the sensor array around the steel rebar. The sensors were therefore placed as ideal as possible. The current layout has the disadvantage that the localisation errors of the events originating from the bottom part of the sample were too high or that they could not be localised at all (e.g. the crack at the bottom of sample A).
Second, for this kind of AE analysis it is very important that the length of the time window of the stored signal is long enough. Also the pre-trigger time is an important setting. A longer pre-trigger time than 20 μs might have been better in order to estimate the real arrival time for more low-amplitude signals, originating from the corrosion itself.
Third, the clustering algorithm was able to cluster different types of signals. However, many signals were assigned to one cluster whereas for the other clusters few signals were recorded. A broadband sensor with a wider frequency range might help to overcome this. However, it was chosen in the current investigation to put the lower limit of the system to 95 kHz as many background noise was captured when this limit was set to 25 or 50 kHz.

5 CONCLUSIONS

In this paper, an AE post-processing protocol was presented as well as a clustering algorithm to distinguish different damage sources during the accelerated corrosion process of small RC prisms. Results show that the damage was localised correctly for a sample with and without stirrup. Clustering and characterisation was evaluated based on crack width measurements, time of arrival, and location. This was compared with an RA-AF analysis. It was found that mainly concrete cracking was recorded and localised. The AE post-processing protocol can be of great value for on-site application of the AE technique. Therefore, this analysis will be upscaled to RC beams in further work .

REFERENCES

[1] Song, H., and Saraswathy, V. 2007. Corrosion monitoring of reinforced concrete structures - a review. *International Journal of Electrochemical Science*; **2**:1–28.

[2] Zaki, A., Chai, H. K., Aggelis, D. G., and Alver, N. 2015. Non-destructive evaluation for corrosion monitoring in concrete: A review and capability of acoustic emission technique. *Sensors*; **15(8)**:19069–19101.

[3] Wevers, M. 1997. Listening to the sound of materials: Acoustic emission for the analysis of material behaviour. *NDT and E International*; **30(2)**:99–106.

[4] Van Steen, C., Pahlavan, L., Wevers, M., and Verstrynge, E. 2019. Localisation and characterisation of corrosion damage in reinforced concrete by means of acoustic emission and X-ray computed tomography. *Construction and Building Materials*; **197**:21–29.

[5] Yoon, D. J., Weiss, W. J., and Shah, S. P. 2000. Assessing damage in corroded reinforced concrete using acoustic emission. *ASCE Journal of Engineering Mechanics*; **126(3)**:273–283.

[6] Kawasaki, Y., Wakadu, T., Kobarai, T., and Ohtsu, M. 2013. Corrosion mechanisms in reinforced concrete by acoutic emission. *Construction and Building MAterials*; **48**:1240–1247.

[7] Leelalerkiet, V., Shimizu, T., Tomoda, Y., and Ohtsu, M. 2005. Estimation of corrosion in reinforced concrete by electrochemical techniques and acoustic emission. *Construction and Building Materials*; **48**:1240–1247.

[8] Marec, A., Thomas, J.-H., and El Guerjouma, R. 2008. Damage characterization of polymer-based composite materials: Multivariable analysis and wavelet transform for clustering acoustic emission data. *Mechanical Systems and Signal Processing*; **22**:1441–1464.

[9] Kravchuk, R., and Landis, E. N. 2018. Acoustic emission-based classification of energy dissipation mechanisms during fracture of fiber-reinforced ultra-high-performance concrete *Construction and Building Materials*; **176**:531-538.

[10] Akaike, H. 1974. Markovian representation of stochastic processes and its application to the analysis of autoregressive moving average processes. *Annals of the Institue of Statistical Mathematics*; **26(1)**:363–387.

[11] Kurz, J. H., Grosse, C. U., and Reinhardt H.-W. 2005. Strategies for reliable automatic onset time picking of acoustic emissions and of ultrasound signals in concrete. *Ultrasonics*; **43**:538-546.

[12] Gollob, S. 2017. Source localization of acoustic emissions using multi-segment paths based on a heterogeneous velocity model in structural concrete. PhD dissertation, ETH Zürich.

[13] Ge, M. 2003. Analysis of source location algorithms: Part II: Iterative methods. *Journal of Acoustic Emission*; **21**:29-51.

[14] Schechinger, B. 2006. Schallemissionsanalyse zur Überwachung der Schädigung von Stahlbeton. PhD dissertation, ETH Zürich.

[15] Li, W., Xu, C., Ho, S. C. M., Wang, B., Song, G. 2017. Monitoring concrete deterioration due to reinforcement corrosion by integrating acoustic emission and fbg strain measurements. *Sensors*; **17**:1–12.

[16] Van Steen, C, Verstrynge, E., Wevers, M., and Vandewalle, L. 2019. Assessing the bond behaviour of corroded smooth and ribbed rebars with acoustic emission monitoring *Cement and Concrete Research*; **120**:176–186.